PNC TN941 76－125

Sodium Vapor Deposition in Annular Within Enclosed Ar Cover Gas Space

November, 1976

Power Reactor and and Nuclear Fuel Development
Corporation Oarai Engineering Center

動力炉・核燃料開発事業団 (Power Reactor and Nuclear Fuel Development Corporation)

This paper was prepared for IAEA IWGFR Specialist's Meeting on "Aerosol Formation, Vapor Deposits and Vapor Trapping" to be held at Cadarache, France on December 13∿15, 1976.

Sodium Vapor Deposition in Annular Within Enclosed Ar Cover Gas Space

Y. Himeno, J. Takahashi, K. Yamamoto, K. Mochizuki and R. Saito

Power Reactor and Nuclear Fuel Development Corporation
Akasaka Tokyo Japan

Abstract

In this paper, the results of a vapor deposition experiment with closely arranged annular walls are presented.

A computer code was first made and sodium vapor deposition caused by argon gas natural convection vapor transfer from the pool surface to the annular were numerically calculated. The numerical results thus obtained were about 1/100 of the experimental vapor deposition rate.

On the other hand, measurement of vapor concentration in argon cover gas space indicated that more than 99.5 % of the sodium dispersed into gas pace was in form of mist.

So, it was infered that deposition process was controlled by mist plating on wall. Further investigation on behavior of mists in cover gas space is necessary for accurate evaluation of the vapor deposition.

1 Introduction

In the Ar cover gas space of a LMFBR, there contained considerable amount of sodium vapor and mists, and these produce operational difficulties of the reactor components such as a rotating plug, a fuel handling machine, a mechanical pump, a vapor trap and so on. To reduce the difficulties, the basic studies have been carried out to date by many investigators. Recently, Kumada et al [1] showed that the evaporated sodium vapor change to mists easily within Ar gas temperature boundary layer above pool surface between 300-400°C into room temperature Ar atomospher. The mists concentration in Ar gas space is reported to be 1-50 g/m^3 within 5.08 cm ID and 20.32 cm length of gas space between 400-450°C sodium pool temperature[2], and these are 100-1,000 times larger than the saturated vapor concentration at its Ar cover gas temperature of about 290°C.

Reviewing these results, it is reasonable to estimate that most fraction of the sodium vapor in Ar gas space are dispersed in the form of sodium mists. However, as to the contribution of the mists behaviour to vapor deposition rate on the wall of the coolant components, quantitative evaluation is not yet established. Because, particle size distribution, mists concentration and some other physical properties which controll mists behavior are not well understood.

In the present paper, experimental results of sodium vapor deposition on annular gap walls are presented. The object of the work was to evaluated the effect of saturated vapor condensation and of mists deposition on over all deposition process. (Here, for distinction, vapor deposition caused by saturated vapor condensation with monomer or dimer will be called "vapor condensation", and that caused by mists wall plating or deposition will be called "mists deposition". What we call "vapor deposition" containes these two processes.) The results of the study include; (1) Measurement of the deposition rate on

annular gap walls with top end closed and bottom end opened with gap width of 10-40 mm and gap axial length of 600 mm,; (2) The development of the computer code to describe the vapor transfer with saturated vapor concnetration based on Ar cover gas natural convection.; and (3) Measurement of the mists concentration in cover gas space.

2 Experimental Arrangement

The sodium loop used in this study is shown in Fig 1. It has three test vessels and these were offered to the present study of the vapor deposition and for the mists concentration measurements. The electrical heaters are provided for adjustment of the sodium temperature at the inlet of the test vessels. The loop also has a cold trap and a plugging indicator for purification and purity monitoring during the experiment.

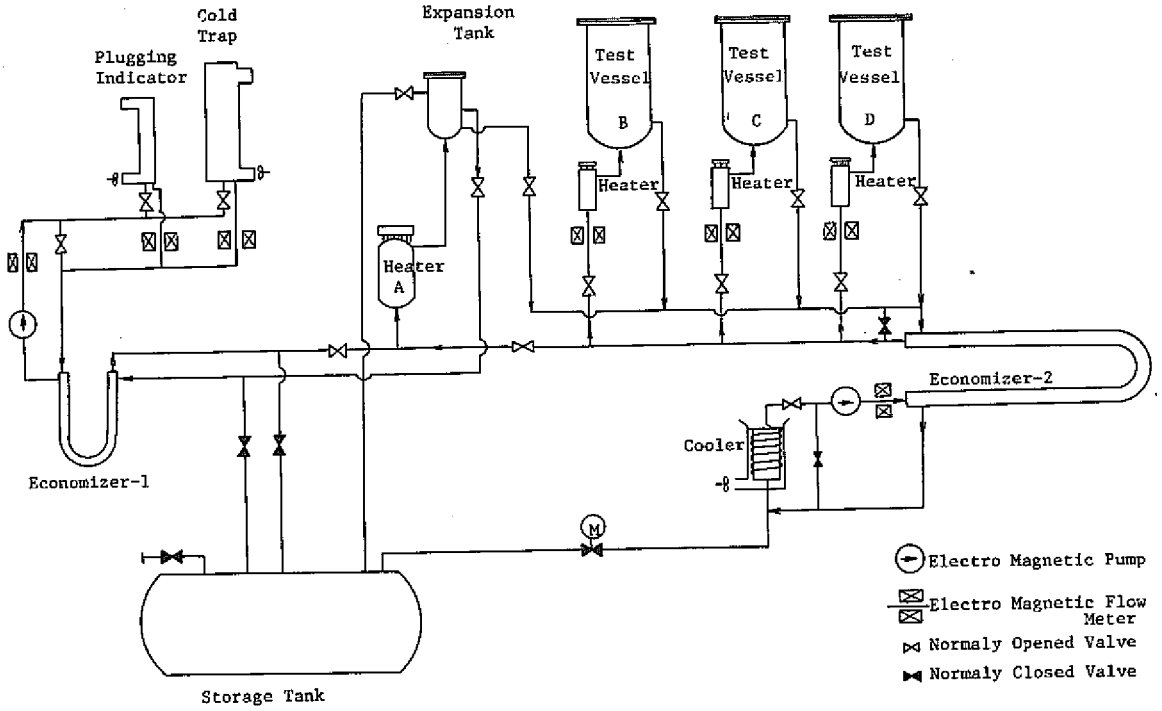

Fig. 1 Flow Sheet of Test Loop

Study of the deposition rate on annular walls were carried out with the arrangement of the test vessel and the test assembly shown in Fig 2. The vessel is of a cylindrical shaped one with its inner diameter of 305.5 mm and longitudial length of 1,800 mm. Its lower about 400 mm was filled with purified flowing sodium and, at its upper half, the test assembly was mounted.

The test assembly were composed with 4 cylinders with their axial length of 600 mm as shown in Fig 2. Each cylinders are different in their diameters and these form different width of annular gap spaces with top end closed and bottom end opened. Such test assemblies were made two. One has 3 annular gaps with width of 10.0, 17.8 and 35.6 mm, and the other has 3 annualr gaps with width of 15.0, 22.8, and 40.6 mm, respectively, for vapor deposition. Former test assembly was designated as /B/ test assembly and the latter was designed as /C/ test assembly.

Along total length of 600 mm across the test assembly, 4 cross section were provided for the temperature measurement at o mm, at 150 mm, at 350 mm and at 530 mm, from the bottom, respectively. Further, the test assembly was designed to be removed and disassembled the part of the annular walls for determination of the amount of deposited sodium on them. Fig 3 shows this for explanation.

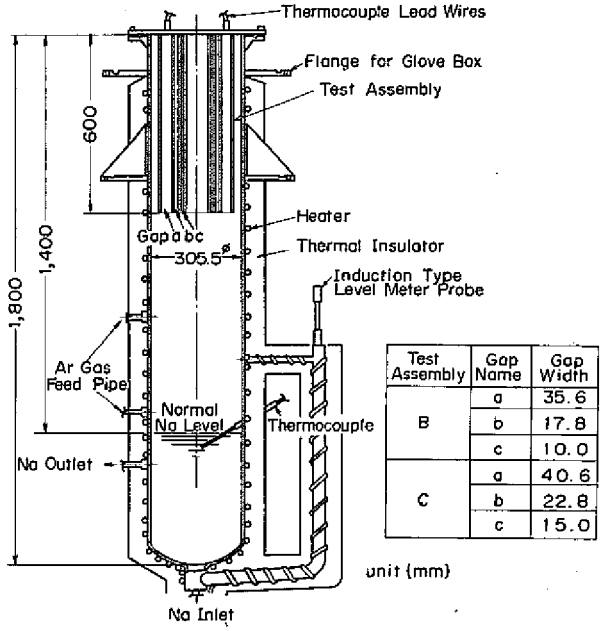

Test Assembly	Gap Name	Gap Width
B	a	35.6
	b	17.8
	c	10.0
C	a	40.6
	b	22.8
	c	15.0

Fig.2 Drawing of Test Vessel and Test Assembly

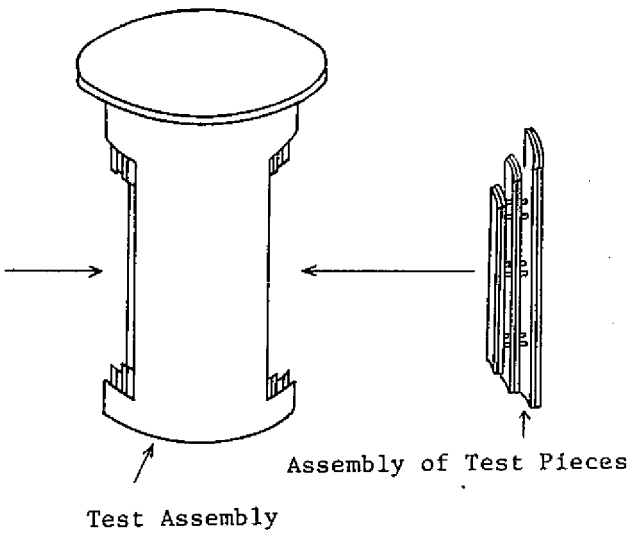

Fig.3 Mounting of Test Pieces to Test Assembly

Measurement of the mists concentration in Ar cover gas space were conducted using the experimental arrangement shown in Fig 4. The vessel was that used for above mentioned experiment for deposition rate. A flange with cover gas exhaust nozzle was attached to the vessel and a mist trap, a back-up filter, a gas cooler and a flow meter were installed in series at the Ar gas down stream positions. These were used for filtration of mists and for Ar gas flow rate measurement. In the mist trap, three stainless steel filters with average filter size with 40, 20, 10 micron, respectively, were installed perpendicular to its flow area. Total filter efficiency of the mists trap was higher than 98 %. Function of the back-up filter was for further collection of the mists in Ar gas stream which could not removed by the mist trap. Glass wool was filled into it.

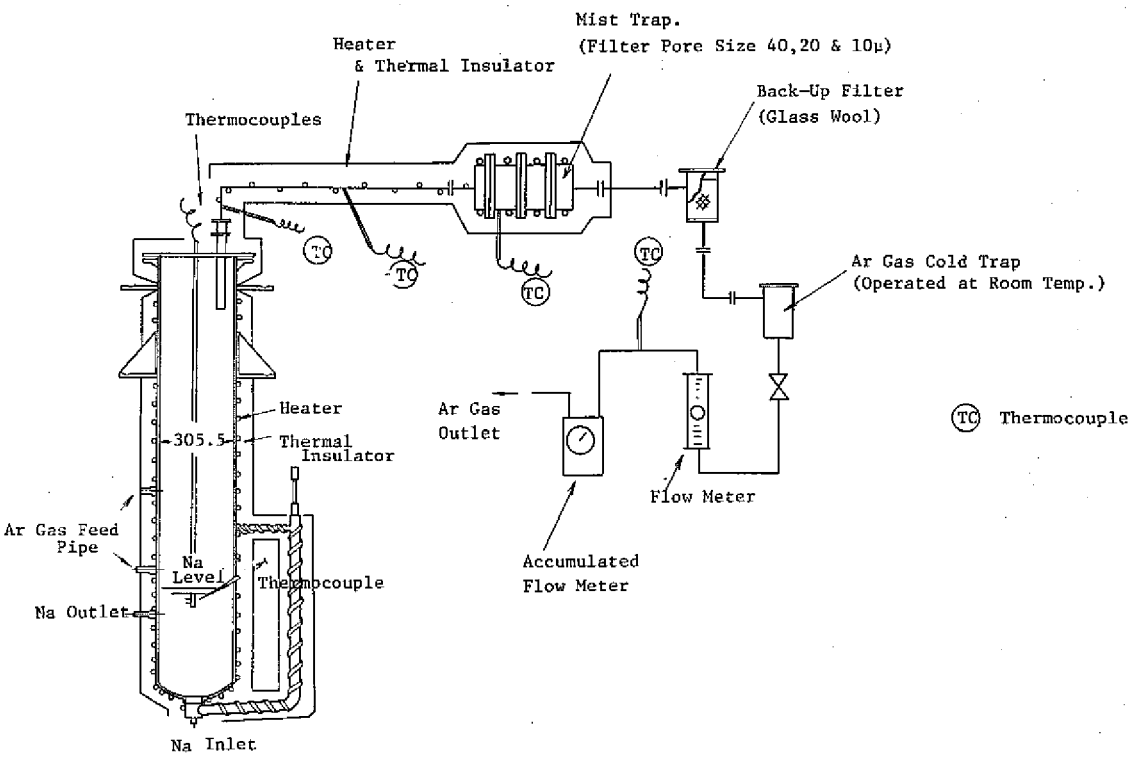

Fig. 4 Flow Sheet of Apparatus for Mists Collection

3 Experimental Procedures

3.1 Deposition Experiment

Fifteen runs were made with experimental conditions tabulated in Tables-1 and 2. Table-1 is for Ar gas pressure with 0.2 kg/cm^{2}G and Table-2 is for Ar cover gas pressure with 1.5 kg/cm^{2}G. Generally, diffusion coefficient of both vapor and mists in gas space is approximately inversely proportional to the system total pressure[3], [4]. So, experiment with these different gas pressure were made to check validity of the obtained data.

Table 1 Experimental Conditions of Series No.1

Run No.	Na Temp.(°C)	Ar Gas Press.(Kg/cm^{2}G)	PM Temp.(°C)	Q(ℓ/min)	t(hrs)
B-400C-20H	400	0.2∿0.3	150	5	20
B-400C-100H	400	0.2∿0.35	"	"	100
C-400C-100H	400	"	"	"	100
B-450C-45H	433	0.2	"	"	45
C-450C-45H	439	"	"	"	45
B-475C-30H	473	"	"	"	30.3
C-475C-30H	475	"	"	"	30.3
B-480C-15H	490	"	"	"	17

Table 2 Experimental Conditions of Series No.2

Run No.	Na Temp.(°C)	Ar Gas Press(Kg/cm^{2}G)	PM Temp.(°C)	Q(ℓ/min)	t(hrs)
C-550C-5H	550	1.5	150	7.5	5.5
B-520C-10H	520	"	"	"	11.0
C-450C-45H	450	"	"	"	45.25
B-430C-90H	430	"	"	"	90
C-500C-13H	500	"	"	"	13
C-470C-30H	470	"	"	"	30
B-450C-45H	450	"	"	"	45

PM Temp. : Plugging Temperature
Q : Na Flow Rate into the Vessel
t : Test Duration

Before entering into the experiment, trail runs were made to obtaine approximate deposition rate. With these, the maximum test duration hours, within which deposited sodium on gap walls are not likely to drop back into the pool surface, were determined as a function of pool temperature. All runs tabulated in Tables-1 and 2 were

carried out within these maximum duration hours.
Surface area of the pool surface oxide film has a intense effect to vapor evaporation rate. So, to avoid uncertainties caused by these surface state, required purification operation hours for complete removal of the surface oxide film was determined viewing the pool surface visually through glass window attached at the top flange of the test vessel. Fig 5 shows a series of the photos which illustrate the change of this surface state as time lapses after sodium filling into the vessel. In the experimental runs, cold trapping of loop sodium were continued for, at least, five hours untill plugging temperature became lower than 150°C. So surface oxide film was completely removed.

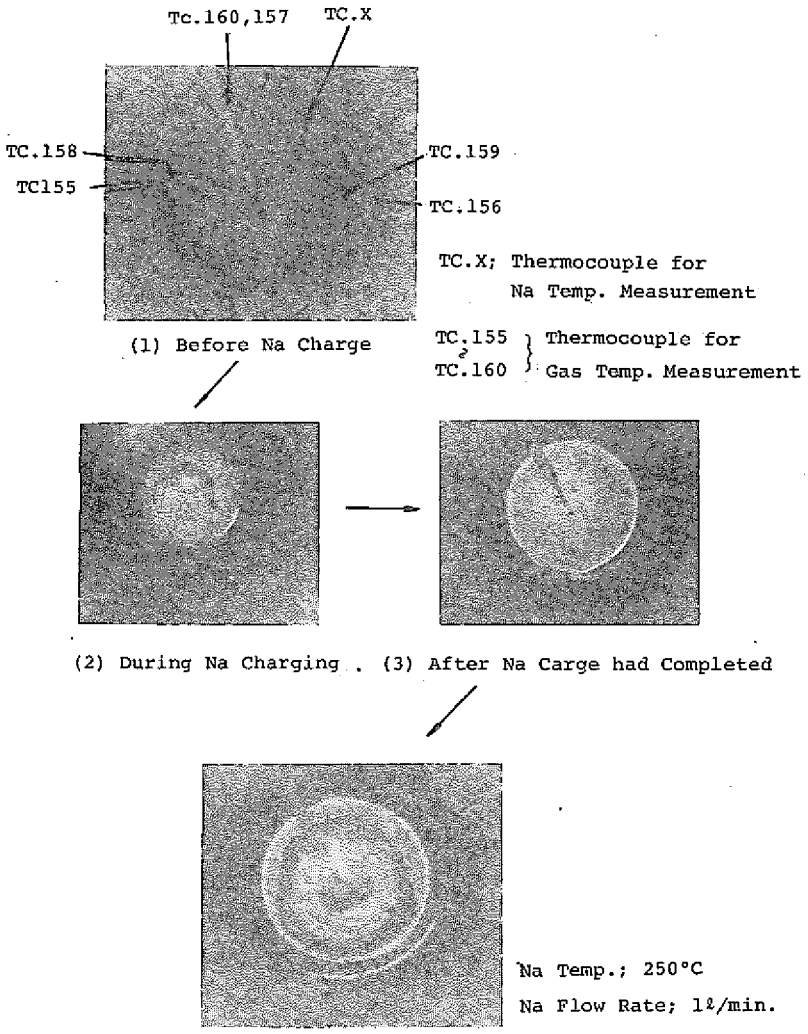

Fig.5 Surface States of the Liquid Sodium in Test Vessel C During Na Charging and Purification Operation

Dismantling of the test assembly after termination of each runs was conducted within the grove box at room temperature. The parts of the annular walls were removed from the test assembly as shown in Fig 3 and these were offered to the measurement of the deposited sodium. In these, the sodium on the parts of the walls were dissolved with ethyalcohol and distilled water. The solution thus obtained was dried on water bath untill attainment of white powder. The powder was changed into sodium-hyroxide solution by adding distilled water and the sodium concentration was determined by titration with standard hydrochloric acid.

3.2 Measurement of Mists Concentration In Cover Gas Space

Five runs were made with experimental conditions tabulated in Table-3, with cover gas pressure of 0.1 kg/cm G, and pool temperatures rages of 360-460°C. Collection of the sodium mists in gas was conducted using the mist trap and the back-up filter by feeding purified Ar gas into the vessel and, thus, exhausing cover gas from it. In these, the mist trap was preheated to higher than 150°C to ensure high removal efficiency for mists collection. Feed Ar gas used was of a commercial grade (higher than 99.9 % purity) and was purified through catalyst filled columm to the pruity of seven-nine.

Determination of the collected mists weight was conducted by removaling each filters and glass wool in the mist trap and back-up filter, respectively. Trapped sodium was dissolved with alcohol and distilled water. The method emplyed for the determination of the sodium concentration was the same as that for deposition experiment described above.

Table 3 Sodium Mists Concentration in Ar Cover Gas Space

Run No.	Pool Temp. (°C)	Temp. of Roof Flange (°C)	Average Gas Temp. (°C)	Mists Concentration at Average Gas Temp. (g/m^3)
51-VM-01-4	440~445	140~167	290~306	2.94
" 3	444	178	311	3.26
" 2	458	180	319	3.88
51-VM-02-1	364	160	262	0.314
" 2	385	170	273	0.603

4 Code for Natural Convection Vapor Transfer

Development of the code was aimed to study cover gas natural convection vapor transfer in cylindrical coordinate system. As is well known, numerical analysis of natural convection with Grashof number grater than 10^4 encounter difficulties. Because, parabolic equation in basic formulas containe non-linear terms with first order derivatives which express the influence of convection, and these terms intruduce serious problems of stability and conservation into the finite-difference scheme. To reduce such difficulties, three-points-central difference approximation was applied to the code to yield non-linear space derivatives of convection terms in basic formulas. This method has been developed by Torrance et al[5], and satisfactory agreement of the computed results with experiment data has also been obtained in natural convection heat transfer experiment conducted by Abe et al[6].

4.1 Formulation of Problem

Consider the motion of Ar gas, in which sodium vapor is contained, within combined spaces of vertical cylinder and annular space shown in Fig 6. Take a origin of the cylindrical coordinates at the center of the bottom. The gas is initially motionless and at a uniform temperature. The problem of the numerical analysis is to find the subsequent velocities, temperatures and sodium vapor densities as function of time and position, and to obtaine the fully developed solution.

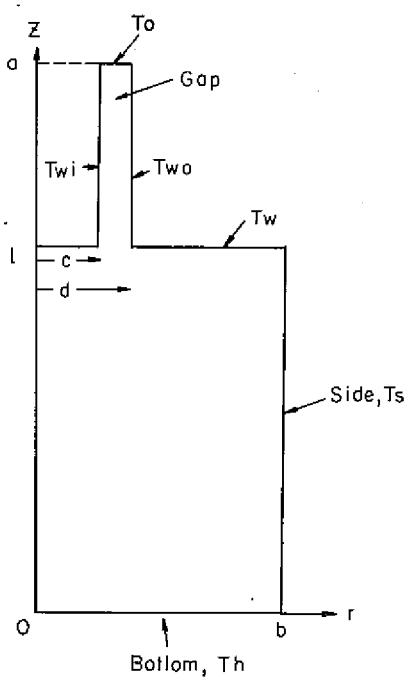

Fig.6 Analytical Coordinate

The Bossinesq approximation is applied to the gas; in this density ρ is assumed constant except for the generation of buoyancy forces, and flow is assumed to be axisymetric. Other fluid properties; kinematic viscosity, thermal diffusivity and volume expansion coefficient are taken as constant.

The basic equations for convection under these assumptions are as follows.

Mass Conservation Eq

$$\mathrm{div}\ \vec{v} = 0 \tag{1}$$

where $\vec{v}$; velocity vector

Momentum Conservation Eq

$$\frac{\partial \vec{v}}{\partial t} + (\vec{v}\nabla)\vec{v} = \vec{K} - \frac{1}{\rho}\mathrm{grad}\ p + \nu\nabla^2\vec{v} \tag{2}$$

where $\vec{K}$; external force vector

ρ; density

ν; kinematic viscosity

t; time

p; system pressure

Energy Conservation Eq

$$\frac{\partial T}{\partial t} + \mathrm{div}\ (T\vec{v}) = \kappa \nabla^2 T \qquad (3)$$

where T; temperature

κ; thermal diffusivity

Eq for Saturated Vapor Transport

$$\frac{\partial w}{\partial t} + \mathrm{div}\ (w\vec{v}) = D\nabla^2 w \qquad (4)$$

where w; vapor fraction

D; diffusion coefficient of sodium vapor in argon cover gas

In trasport requation of (4), only vapor transfer with saturated vapor density is considered. Transfer with sodium mists is omitted. For formulation of above five Eqs in cylindrical coordinates system, dimentionless vorticity vector was introduced.

$$\vec{\Omega} = rot\ \vec{v} \qquad (5)$$

where $\vec{\Omega}$; dimentionless vorticity vector

Eq. (5) could be expressed as follow, since the flow assumed to be axisymmetric, therefore, dimentionless vorticity vector has only azimuthal component.

$$\Omega = (-\frac{\partial u}{\partial r} + \frac{\partial v}{\partial z}) \qquad (6)$$

where u : radial component of velocity

v : vertical component of velocity

Further, mass conservation eq. of (1) is automatically satisfied by intorudcing of a dimentionless stream function ψ

$$u=\frac{1}{r}\frac{\partial\psi}{\partial r},\quad v=-\frac{1}{r}\frac{\partial\psi}{\partial z} \tag{7}$$

The momentum conservation eq. of (2) is converted into the equation for vorticity by taking its rotation, and yields the following eq.

$$\rho\frac{\partial\Omega}{\partial t}+\rho\left\{\frac{\partial}{\partial r}(v\Omega)+\frac{\partial}{\partial z}(u\Omega)\right\}=\rho g\beta(T-T_1)\frac{\partial T}{\partial r}+\rho\nu\left\{\frac{1}{r}\frac{\partial}{\partial r}\left(\frac{1}{r}\frac{\partial\Omega}{\partial r}\right)+\frac{\partial^2\Omega}{\partial z^2}\right\} \tag{8}$$

In a similar way, we obtaine Eqs. (9) and (10) from eq of energy conservation of (3) and eq. of vapor transpor of (4), respectively.

$$\frac{\partial T}{\partial t}+\frac{\partial(uT)}{\partial z}+\frac{1}{r}\frac{\partial(rvT)}{\partial r}=\kappa\left\{\frac{1}{r}\frac{\partial}{\partial r}\left(r\frac{\partial T}{\partial r}\right)+\frac{\partial^2 T}{\partial z^2}\right\} \tag{9}$$

$$\frac{\partial w}{\partial t}+\frac{1}{r}\frac{\partial}{\partial r}(rvw)+\frac{\partial}{\partial z}(uw)=D\left\{\frac{1}{r}\frac{\partial}{\partial r}\left(r\frac{\partial w}{\partial r}\right)+\frac{\partial^2 w}{\partial z^2}\right\} \tag{10}$$

Eqs. (6), (7), (8), (9) and (10)are the basic equations for natural convection in axisymetric cylindrical coordinates system. These five basic equations were further generalized with following dimentionless quantities;

$\tau=\frac{k}{a^2}t$; time

$Z=z/a$; vertical coordinate

$R=r/a$; radial coordinate

$V=\frac{a}{\kappa}v$; vertical component of velocity

$U=\frac{a}{\kappa}u$; radial componnet of velocity

$\theta = \frac{T - To}{Th - To}$; temperature

Th ; hot surface temp;

To; cold surface temp

Φ ; stream function

Ω ; vorticity

$W = \frac{w - w_o}{w_u - w_o}$; vapor fraction

By introducing these dimentionless quantities into above five basic equations, the following equations are derived and these contain the Grashof number and Prandtle number.

$$G_r = \frac{g\beta (T_h - T_o) a^3}{\nu^2}, \quad P_r = \frac{\nu}{\kappa}, \quad \nu = \frac{\mu}{\rho}, \quad \kappa = \frac{\lambda}{c\rho g}$$

Velocity Eq

$$U = \frac{1}{R}\frac{\partial \Phi}{\partial R}, \quad V = -\frac{1}{R}\frac{\partial \Phi}{\partial Z} \tag{11}$$

Eq of Stream Function

$$-\Omega = \frac{\partial}{\partial R}\left(\frac{1}{R}\frac{\partial \Phi}{\partial R}\right) + \frac{1}{R}\frac{\partial^2 \Phi}{\partial Z^2} \tag{12}$$

Vorticity Eq

$$\frac{\partial \Omega}{\partial \tau} + \frac{\partial}{\partial R}(V\Omega) + \frac{\partial}{\partial Z}(U\Omega) = -G_r P_r^2 \frac{\partial \theta}{\partial R} + P_r\left\{\frac{\partial}{\partial R}\left(\frac{1}{R}\frac{\partial (R\Omega)}{\partial R}\right) + \frac{\partial^2 \Omega}{\partial Z^2}\right\} \tag{13}$$

Energy Conservation Eq

$$\frac{\partial \theta}{\partial \tau} + \frac{\partial (U\theta)}{\partial Z} + \frac{1}{R}\frac{\partial (RV\theta)}{\partial R} = \frac{\partial^2 \theta}{\partial Z^2} + \frac{1}{R}\frac{\partial}{\partial R}\left(R\frac{\partial \theta}{\partial R}\right) \tag{14}$$

Transport Eq of Saturated Vapor

$$\frac{\partial W}{\partial \tau}+\frac{\partial (UW)}{\partial Z}+\frac{1}{R}\frac{\partial (RVW)}{\partial R}=\left(\frac{P_r}{S_c}\right)\left\{\frac{1}{R}\frac{\partial}{\partial R}\left(R\frac{\partial W}{\partial R}\right)+\frac{\partial^2 W}{\partial Z^2}\right\} \tag{15}$$

4.2 Finite Difference Scheme

Non-linear terms of space derivations such as $\partial(U\theta)/\partial Z$, $\partial(RV\theta)/\partial R$, $\partial(U\Omega)/\partial Z$ and $\partial(VR)/\partial R$ were approximated by three-point-central-difference method. As an example, approximation of $\partial(U\theta)/\partial Z$ will be explained here.

In mesh points and cell boundary shown in Fig 7, Z-component of velocity at points $(i-\frac{1}{2}\cdot j)$ and $(i+\frac{1}{2}\cdot j)$ can be approximated as follows.

$$\text{at} \quad (i-\frac{1}{2},j) \quad U_{i-\frac{1}{2},j}=\frac{U_{i-1,j}+U_{ij}}{2}$$

$$\text{at} \quad (i+\frac{1}{2},j) \quad U_{i+\frac{1}{2},j}=\frac{U_{i,j}+U_{i+1,j}}{2}$$

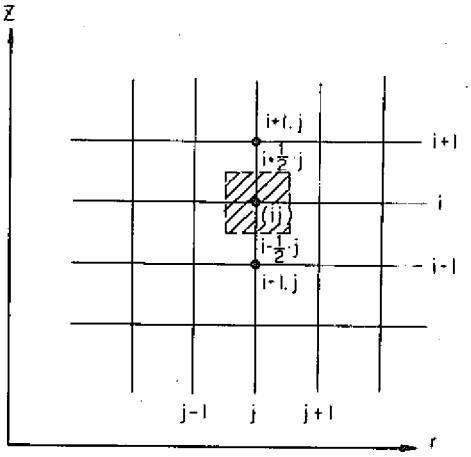

Fig.7 Mesh Points and Cell Boundary

For approximation of $\partial(U\theta)/\partial Z$,
it is assumed that quantity of U enters into point (i.j) with $(U_{i-1\cdot j}+U_{i\cdot j})\theta_{i-1\cdot j/2}$ from point $(i-\frac{1}{2}\cdot j)$ and goes out with $(U_{i+1\cdot j}+U_{i\cdot j})\theta_{i\ j/2}$ into point $(i+\frac{1}{2}\cdot j)$, when Z-component of velocity is positive. In this, temperature variation around (i·j) point is assumed to be very mild,

so, approximation of $\partial(U\theta)/\partial Z$ could be expressed by Eq (16), when U>0

$$\left\{\frac{\partial(U\theta)}{\partial Z}\right\}_{i,j}=\frac{1}{\Delta Z}\left\{\frac{U_{i+1,j}+U_{i,j}}{2}\theta_{i,j}-\frac{U_{i,j}+U_{i-1,j}}{2}\theta_{i-1,j}\right\} \tag{16}$$

$$U>0$$

On the other hand, when Z-component of velocity is negative, and fluid flows downward in Fig 7, the approximation of $\partial(U\theta)/\partial Z$ yield eq (17)

$$-\left\{\frac{\partial(U\theta)}{\partial Z}\right\}_{i,j}=\frac{1}{\Delta Z}\left\{\frac{U_{i,j}+U_{i-1,j}}{2}\theta_{i,j}-\frac{U_{i+1,j}+U_{i,j}}{2}\theta_{i+1,j}\right\} \tag{17}$$

$$U<0$$

When, the approximation similar to Eqs.(16) and (17) is applied to the vorticity Eq.(13), their non-linear space derivatives can be approximated as Eqs.(18) and (19), when sign of all velocity componebts are positive,

$$\frac{\partial}{\partial R}(V\Omega)_{i,j}=\frac{1}{\Delta R}\left\{\frac{V_{i,j+1}+V_{i,j}}{2}\Omega_{i,j}-\frac{V_{ij}+V_{i,j-1,}}{2}\Omega_{i,j-1}\right\} \tag{18}$$

$$\frac{\partial}{\partial R}(V\Omega)_{i,j}=\frac{1}{\Delta R}\left\{\frac{V_{i+1,j}+U_{i,j}}{2}\Omega_{i,j}-\frac{V_{i,j}+U_{i-1,j}}{2}\Omega_{i-1,j}\right\} \tag{19}$$

Other differential terms in Eq.(13) were approximated by finite difference approximation.

$$\left(\frac{\partial^2\Omega}{\partial\tau^2}\right)_{i,j}=\frac{\Omega_{i+1,j}-2\Omega_{i,j}+\Omega_{i-1,j}}{2} \tag{20}$$

$$-G_rP_r^2\left(\frac{\partial\theta}{\Delta R}\right)_{i,j}=-G_rP_r^2\frac{\theta_{i,j+1}-\theta_{i,j-1}}{2\Delta R} \tag{21}$$

$$\left(\frac{\partial\Omega}{\partial\tau}\right)_{i,j}=\frac{\Omega'_{i,j}-\Omega_{i,j}}{\Delta\tau} \tag{22}$$

where, $\Omega'i\cdot j$; vorticity function at $\tau' = \Delta\tau+\tau$

$\Omega i\cdot j$; " at $\tau = \tau$

By substituting Eqs (18)-(22) into Eq (13), approximation of vorticity equation became as follows

$$\frac{\Omega'_{i,j}-\Omega_{i,j}}{\Delta\tau}+\frac{(U_{i+1,j}+U_{i,j})\Omega_{i,j}-(U_{i,j}+U_{i-1,j})\Omega_{i-1,j}}{2\Delta Z}$$

$$+\frac{(V_{i,j+1}+V_{i,j})\Omega_{i,j}-(V_{i,j}+V_{i,j-1})\Omega_{i,j-1}}{2\Delta R}=-G_r P_r^2\frac{\theta_{i,j+1}-\theta_{i,j-1}}{2\Delta R}$$

$$+P_r\frac{\Omega_{i+1,j}-2\Omega_{i,j}+\Omega_{i-1,j}}{\Delta Z^2}+\frac{\left(\frac{j+1}{j+\frac{1}{2}}\right)\Omega_{i,j+1}-\left(\frac{j}{j+\frac{1}{2}}+\frac{j}{j-\frac{1}{2}}\right)\Omega_{i,j}+\left(\frac{j-1}{j-\frac{1}{2}}\right)\Omega_{i,j-1}}{(\Delta R)^2} \quad (23)$$

With quite similar way, Eqs for energy conservation (14) and for saturated vapor transport (15) yield following Eqs.

$$\frac{\theta'_{i,j}-\theta_{i,j}}{\Delta\tau}+\left(-\frac{U_{i+1,j}+U_{i,j}}{2}\theta_{i,j}-\frac{U_{i,j}+U_{i-1,j}}{2}\theta_{i-1,j}\right)\frac{1}{\Delta Z}$$

$$+\frac{(j+\frac{1}{2})(V_{i,j+1}+V_{i,j})\theta_{i,j}-(j-\frac{1}{2})(V_{i,j}+V_{i,j-1})\theta_{i,j-1}}{2j\Delta R}=\frac{\theta_{i+1,j}-2\theta_{i,j}+\theta_{i-1,j}}{\Delta Z^2}$$

$$+\frac{(j+\frac{1}{2})\theta_{i,j+1}-2j\theta_{i,j}+(j-\frac{1}{2})\theta_{i,j-1}}{j\Delta R^2} \quad (24)$$

$$\frac{W'_{i,j}-W_{i,j}}{\Delta\tau}+\left(\frac{U_{i+1,j}+U_{i,j}}{2}W_{i,j}-\frac{U_{i,j}+U_{i-1,j}}{2}W_{i-1,j}\right)\frac{1}{\Delta Z}$$

$$+\frac{(j+\frac{1}{2})(V_{i,j+1}+V_{i,j})W_{i,j}-(j-\frac{1}{2})(V_{i,j}+V_{i,j-1})W_{i,j-1}}{2j\Delta R}$$

$$=\left(\frac{P_r}{S_c}\right)\left\{\frac{W_{i+1,j}-2W_{i,j}+W_{i-1,j}}{\Delta Z^2}+\frac{(j+\frac{1}{2})W_{i,j+1}-2jW_{i,j}+(j-\frac{1}{2})W_{i,j-1}}{j\Delta R^2}\right\} \quad (25)$$

At the centerline with R=0, special forms of Eq (24) and (25) are used which incorporate boundary conditions of Eq (41).

$$\Omega_{i,0} = O \tag{26}$$

$$\frac{\theta'_{i,0} - \theta_{i,0}}{\Delta\tau} + \frac{1}{\Delta Z}\left\{\frac{U_{i+1,0}+U_{i,0}}{2}\,\theta_{u(i),0} - \frac{U_{i,0}+U_{i-1,0}}{2}\,\theta_{l(i),0}\right\} + \frac{2V_{i,1}}{\Delta R}\,\theta_{i,0}$$

$$= \frac{\theta_{i+1,0} - 2\theta_{i,0} + \theta_{i-1,0}}{\Delta Z^2} + \frac{4(\theta_{i,1} - \theta_{i,0})}{\Delta R^2} \tag{27}$$

$$\frac{W'_{i,0} - W_{i,0}}{\Delta\tau} + \frac{1}{\Delta Z}\,\frac{U_{i+1,0}+U_{i,0}}{2}\,W_{u(i),0} - \frac{U_{i,0}-U_{i-1,0}}{2}\,W_{l(i),0} + \frac{2V_{i,1}}{\Delta R}W_{i,0}$$

$$= \left(\frac{P_r}{S_c}\right)\left\{\frac{W_{i+1,0} - 2W_{i,0} + W_{i-1,0}}{\Delta Z^2} + \frac{4(W_{i,1} - W_{i,0})}{\Delta R^2}\right\} \tag{28}$$

$$\Phi_{i,0} = O \tag{29}$$

$$U_{i,0} = \frac{2\Phi_{i,1}}{\Delta R^2} \tag{30}$$

$$V_{i,0} = O \tag{31}$$

Eqs (23),(24),(25),(26),(27),(28),(29),(30) and (31) permit $\theta'_{i,j}$ $W'_{i,j}$ and $\Omega'_{i,j}$ at all mesh points to be explicitly calculated in terms of known quantities.

The new vorticities $\Omega'_{i,j}$ are next introduced into Eq. of stream function (12), which is solved for the new stream function field by successive over-relaxiation method. Thus, if $\Phi_{i,j}^{(s)}$ denotes the approximate stream function at (i,j) point after S-iterations further approximation $\Phi_{i,j}^{(s+1)}$ is obtained from Eq (32) which derived from Eq (12)

$$\Phi_{i,j}^{(s+1)} = \Phi_{i,j}^{(s)} + \omega\left\{\Phi_{i,j}^{(s+1)} - \Phi_{i,j}^{(s)}\right\}$$

$$= (1-\omega)\,\Phi_{i,j}^{(s)} + \frac{\omega}{M}N \tag{32}$$

where

$$M = \frac{2}{\Delta Z^2} + \frac{1}{\Delta R^2}\left(\frac{j}{j+\frac{1}{2}} + \frac{j}{j-\frac{1}{2}}\right)$$

$$N = j\Delta R\Omega_{i,j} + \frac{1}{\Delta Z^2}\left(\Phi^{(s)}_{i+1,j} + \Phi^{(s+1)}_{i-1,j}\right) + \frac{1}{\Delta R^2}\left\{\frac{j}{j+\frac{1}{2}}\Phi^{(s)}_{i,j+1} + \frac{j}{j-\frac{1}{2}}\Phi^{(s-1)}_{i,j-1}\right\} \quad (33)$$

ω; relaxation parameter

For calculation of vorticities along top, bottom and side walls, vorticity function Φ was expanded in Taylor series and Eqs (34)-(38) were derived, using boundary conditions that Φ and its normal derivative are zero.

$$\Omega_{0,j} = -\frac{8\Phi_{1,j} - \Phi_{2,j}}{2(j\Delta R)(\Delta Z^2)} \quad (34)$$

$$\Omega_{N,j} = -\frac{8\Phi_{N-1,j} - \Phi_{N-2,j}}{2(j\Delta R)\Delta Z^2} \quad (35)$$

$$\Omega_{i,M} = \frac{8\Phi_{i,M-1} - \Phi_{i,M-2}}{2j\Delta R^3} \quad (36)$$

$$\Omega_{i,j} = -\left\{\frac{8\Phi_{i-1,j} - \Phi_{i-2,j}}{2j\Delta R\Delta Z^2} + \frac{8\Phi_{i,j+1} - \Phi_{i,j+2}}{2j\Delta R^3}\right\} \quad (37)$$

where $i\Delta Z = \ell$, $j\Delta R = c$

$$\Omega_{i,j} = -\left\{\frac{8\Phi_{i-1,j} - \Phi_{i-2,j}}{2j\Delta R\Delta Z^2} + \frac{8\Phi_{i,j-1} - \Phi_{i,j-2}}{2j\Delta R^3}\right\} \quad (38)$$

where $i\Delta Z = \ell$, $j\Delta R = d$

4.3 Boundary Conditions

(1) Initial Conditions

The fluid is initialy motionless and uniform temperature

$$\tau \leq 0$$

$$0 < Z < 1 \ , \ 0 < R < R_b \left(= \frac{b}{a} \right) \tag{39}$$

$$\Omega = \theta = W = 0$$

(2) Boundary Conditions

At certain time with $\tau > 0$, following boundary conditions were introduced,

$$\left.\begin{array}{l} \text{at} \quad Z = Z_e \ , \ R_d < R < R_b \ , \ R < R_c \\ \qquad \Phi = \dfrac{\partial \Phi}{\partial Z} = 0 \ , \ \theta = \theta_w \ , \ W = W_w \\ \text{at} \quad Z = 0 \ , \ 0 \leq R \leq R_b \quad \Phi = \dfrac{\partial \Phi}{\partial Z} = 0 \ , \ \theta = 1 \ , \ W = 1 \\ \text{at} \quad Z = 1 \ , \qquad\qquad \Phi = \dfrac{\partial \Phi}{\partial Z} = \theta = W = 0 \end{array}\right\} \tag{40}$$

$$\left.\begin{array}{l} \text{at} \quad R = 0 \ , \ 0 \leq R \leq R_b \quad \Phi = \Omega = \dfrac{\partial \theta}{\partial R} = \dfrac{\partial W}{\partial R} = 0 \\ \text{at} \quad R = R_b \qquad 〃 \qquad \Phi = \dfrac{\partial \Phi}{\partial R} = 0 \\ \qquad\qquad\qquad\qquad\quad \theta = \theta_w \ , \ W = W_w' \\ \text{at} \quad Z_e < Z < 1 \ , \ R = R_c \quad \Phi = \dfrac{\partial \Phi}{\partial R} = 0 \\ \qquad 〃 \ , \ R = R_d \qquad 〃 \end{array}\right\} \tag{41}$$

5 Results and Discussion

5.1 Vapor Deposition Rate

Fig 8 shows the experimental data taken. It consists of a plot of average upward vapor deposition flux ϕ across the inlet of three annular gaps of the test assembly vs saturated vapor pressure at sodium pool temperature. ϕ was given by equation (42), and its physical meaning is the effective vapor and mists flux which realy deposited on all annular surfaces of the test assembly. So, it is proportional to the vapor deposition rate.

$$\phi = \frac{\sum_i W_i}{\sum_i S_i t} \tag{42}$$

where W_i ; weight of deposited sodium on annular surface i (i=1,2,...,6). (g)

S_i ; cross section of annular gap space (cm^2) (i=1.2.3)

t ; experiment duration time (sec)

It is known that ϕ increase with saturated vapor pressure at pool temperature. Increase in cover gas pressure resulted in expected decrease in ϕ, and mean ratio of the rate at 0.2kg/cm^2G to that at 1.5kg/cm^2G is 2. This cover gas pressure dependence of the deposition rate is reasonable, since the pressure ratio is approximately equal to 2.

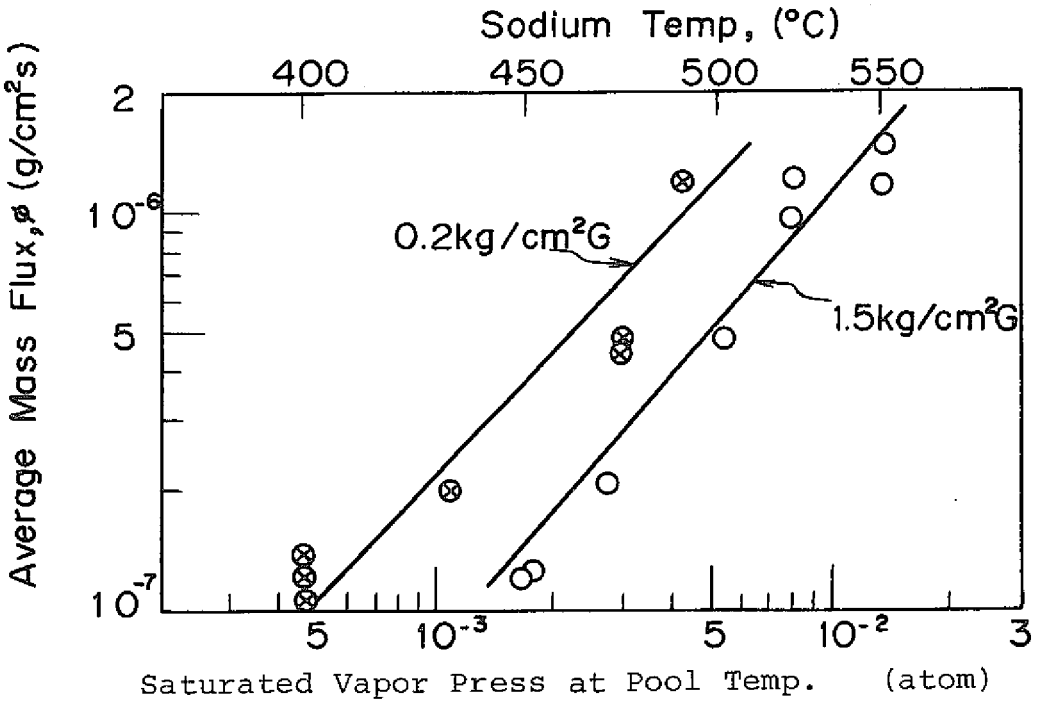

Fig.8 Data of Average Deposited Vapor Flux vs. Saturated Vapor Pressure at Pool Temperature

As to the axial changes of the vapor deposition rate, the results shown in Fig 9 was obtained. The plot is expressed in terms of dimentionless deposition rate vs axial length from inlet of the annular space. In these, exponential decrease in deposition rate is shown as the increase in the distance from the inlet.

The temperature drop across the axial length of the annular surface during the experiment were comparatively large as the order of 100-160°C. Under these higher temperature drop, the difference in saturated vapor pressure at the inlet and at the top of the gap became order of 10^2. So, if it is assumed that the measured deposition rate were controlled by the saturated vapor transfer, the deposition rate should differ for factor of 10^2. However, obtained deposition rate data differ only for factor of 2-10. This would probably attributed to other effect than vapor condensation.

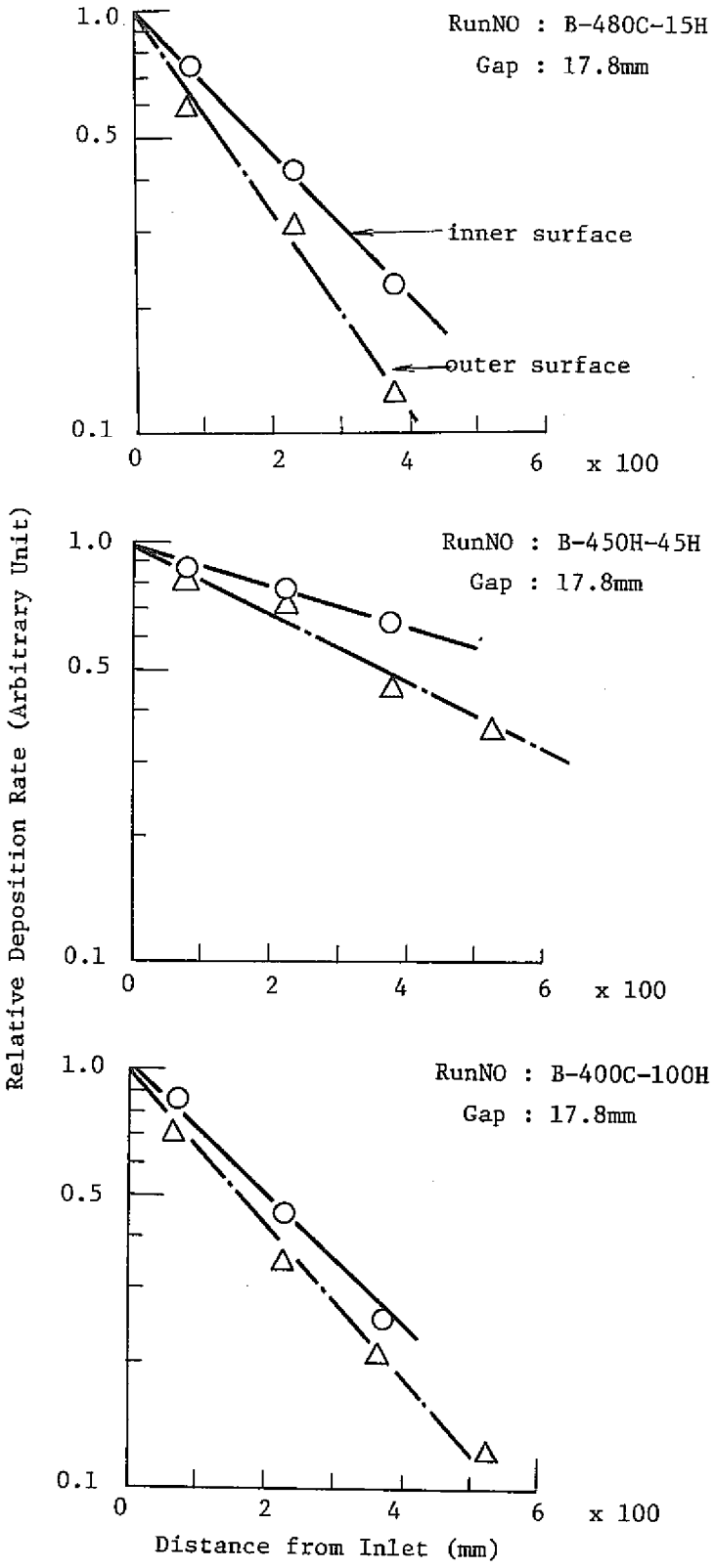

Fig. 9 Distribution of Deposition Rate Along Annular Surface

5.2 Evaluation of Saturated Vapor Condensation

To evaluate saturated vapor condensation rate on annular surface of the test assembly more clearly the computer code described above was used. Object of the analysis was to compare the numerical results with that of the above depostion data, and examine the effect of vapor condensation.

At first, analysis of the convection with the geometry which is consisted with two spaces, one with a annular space and the other one with large space between pool surface and the bottom of the test assembly were conducted. With this geometry, local vapor condensation rate along axial length of the annular surface were calculated. Next, analysis of convection with only one annular space geometry were conducted, and local vapor condensation rate was also calculated. Using the results from these analysis with different geometry, interference of convection between large space and the annular space were examined.

The results of analysis with two space geometry are shown in Figs 10 and 11 with transient temperature θ, stream function Φ and vorticity Ω. Boundary conditions used were experimental temperature data obtained with Run on B-475C-30H, in Table-1, and the annular space considered was b gap (17.8 mm) in B test assembly shown in Fig 2. It is known from Figs 10 and 11 that the temperature field in the annular space dose not change so much as time lapses. Local vapor condensation rate numericaly calculated are shown in Fig 12 with experimentary determined vapor deposition rate with Run no B-475C-30H.

With the similar way, the anlsysis of natural convection within b gap of B test assembly were conducted with simple analytical geometry, in wich only b annular space was taken into account. Then, local vapor condensation rate shown in Fig 12 were obtained.

These numerically calculated results with different analytical geometry are similar to rach other and interference

of the convection between alrge space and the narrow space is known to be negligibly small. However, numerical data are about 2-order smaller than experimentary determiend vapor deposition rate. This means that, in the present experimental system, contribution of vapor condensation to the real vapor deposition process is very small (less than 1 %.)

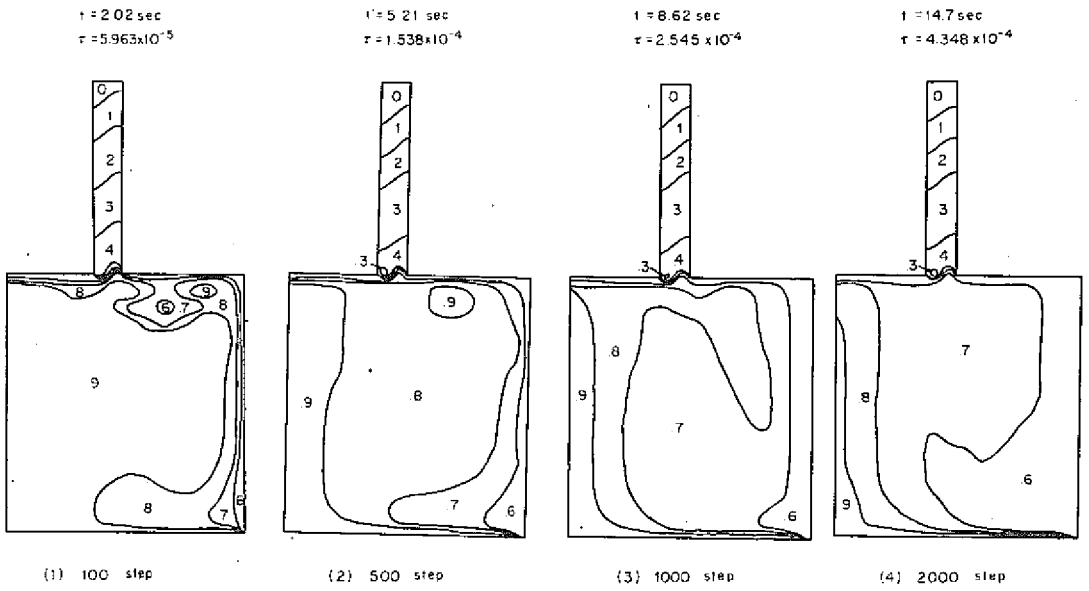

Fig.10 Transient Temperature θ Distibutions in 17.8mm Gap and Free Space in the Vessel (B-475C-30H)

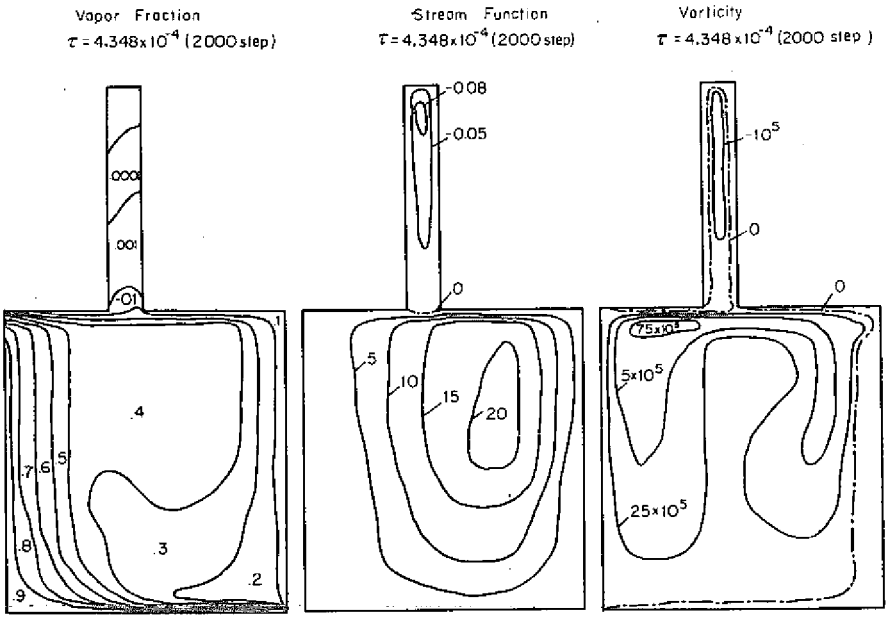

Fig.11 Steady State Vapor Fraction W, Stream Function Φ and Vorticity Ω in 17.8 mm Gap and Free Space

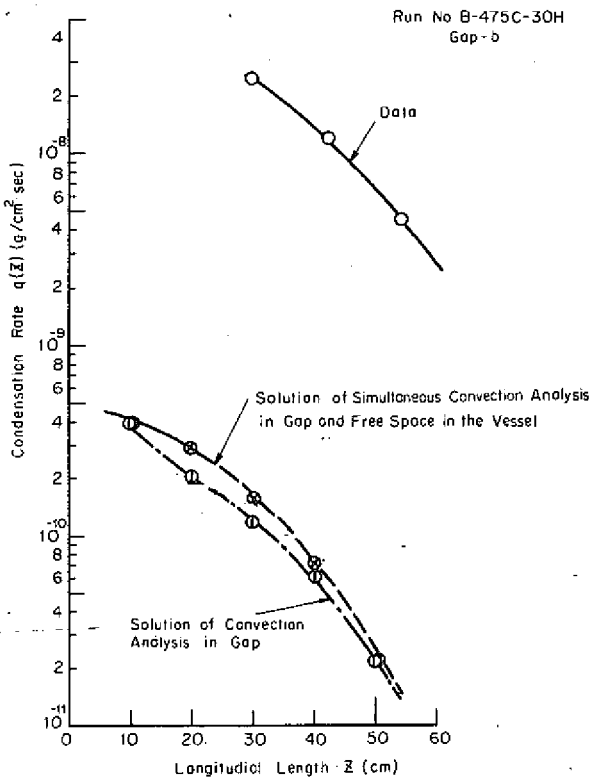

Fig.12 Vapor Condensation Rate q(Z) in 17.8 mm Gap
−Comparison of Data and Numerical Solutions−

5.3 Sodium Mists Concentration in Cover Gas Space

From experimental and numerical data presented above, mists concentration in cover gas space was estimeated to be very high. To investigate this, measurement was carried out and the results shown in Fig 13 were obtained.

Sodium pool temperatures ranges for this measurement were 360-460°C, and the measured concentrations are 0.3 to 4g/m^3. Saturated vapor concentration at pool temperatrues are also plotted in the same Fig. It is known that measured concentrations are about 5 times higher than saturated one. In addition, if these data were compared with saturated vapor concentration at average cover gas temperature above pool surface, the difference became much larger as about 200 times as shown in Fig 14.

In the present study, the temperature difference between pool surface and cover gas were 100-200°C in both cases for mists concentration measurement and vapor deposition experiment described ealier so that temperature conditions for mists formation were similar to each other. Further, Sheth[7] showed in his numerical study of mists behavior that cover gas natural convection current dose not controll the mists concentration. So, present concentration data of Fig 13 permits estimation that the quite the same amount of mists would also dispersed in cover gas space of experimental arrangement for vapor deposition shown in Fig 2, and larger vapor deposition rate presented in Fig 12 would probably attributed to mists deposition.

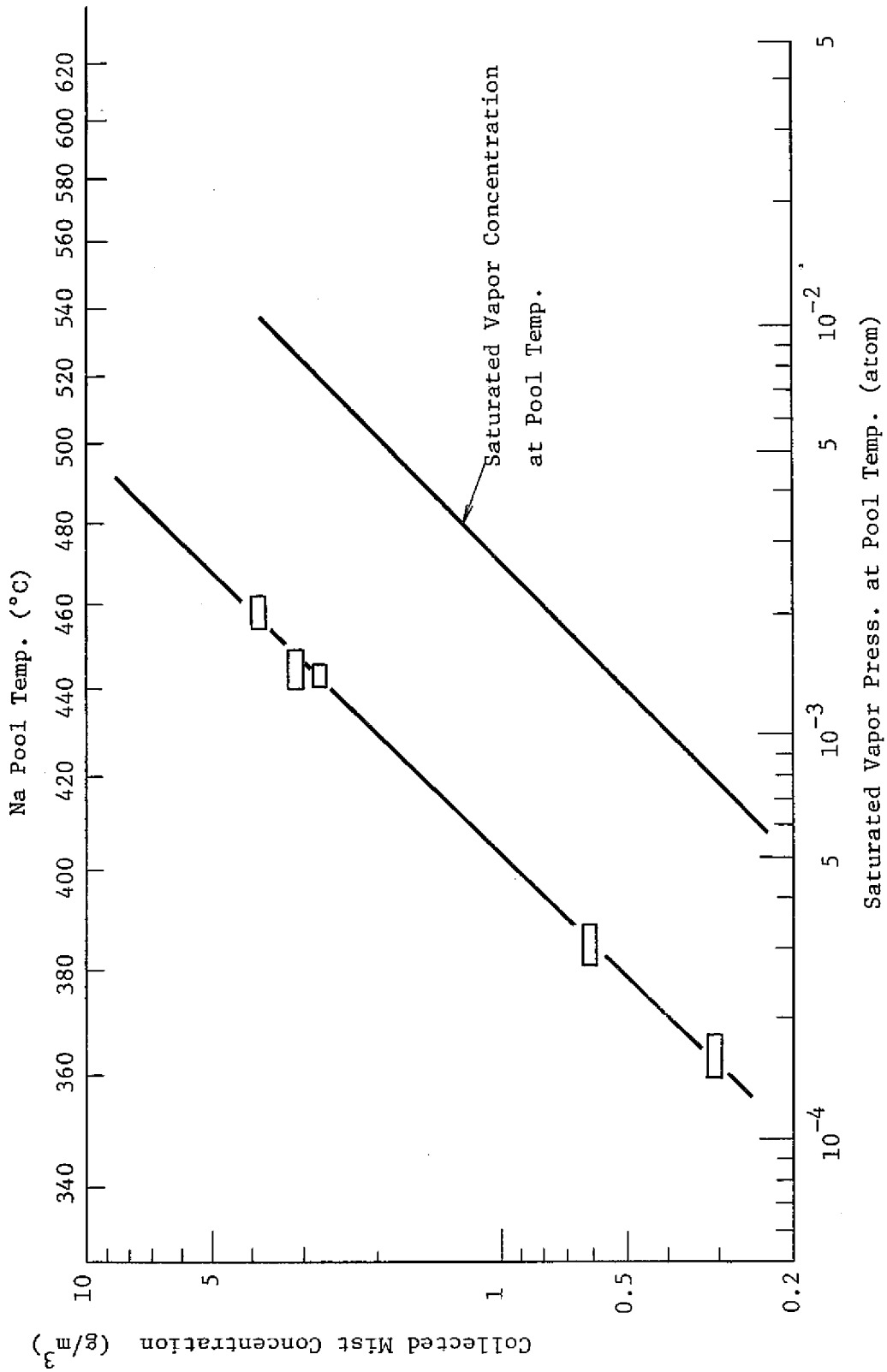

Fig. 13 Collected Sodium Mist Concentration

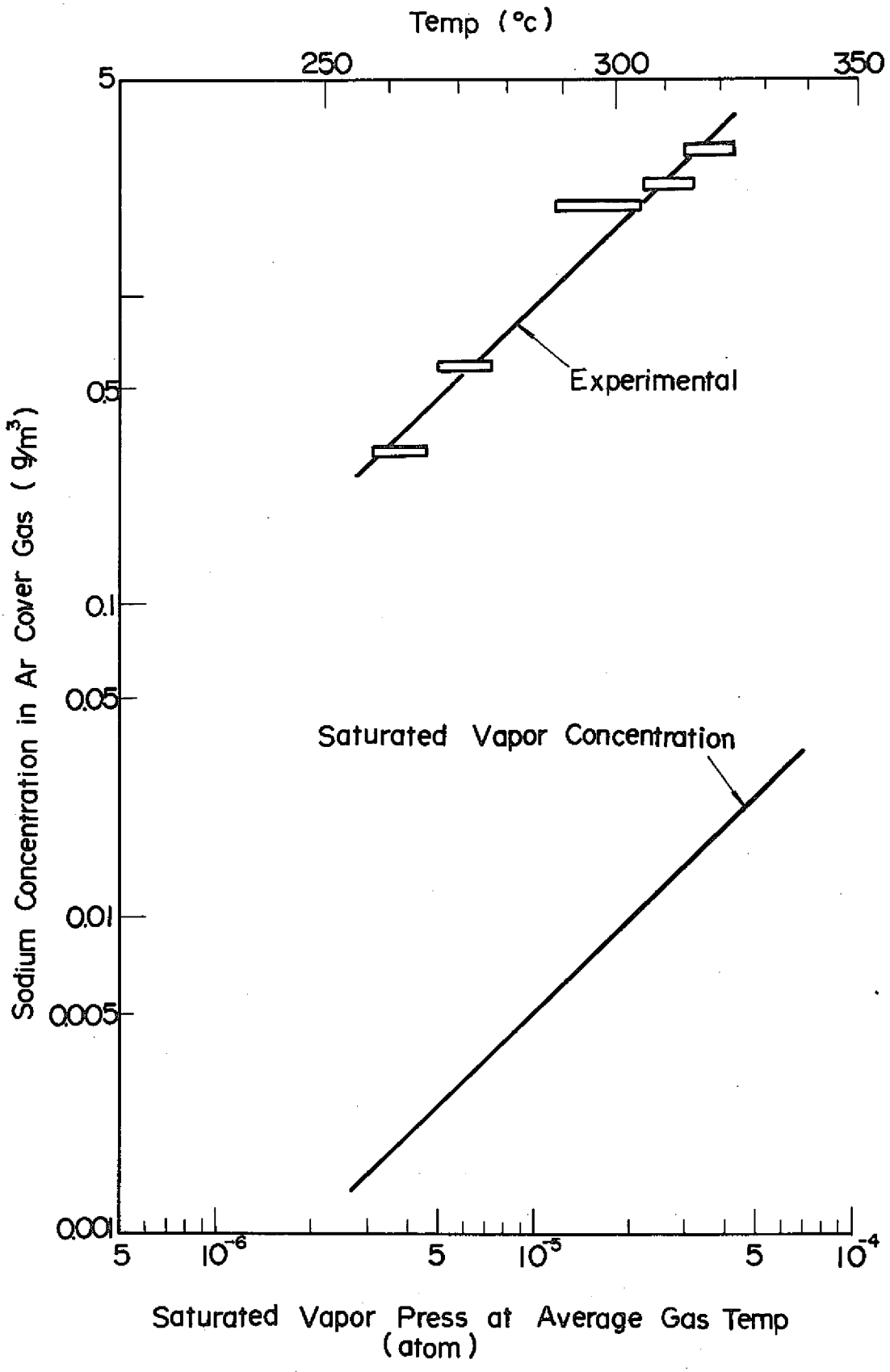

Fig.14 Comparison of Mists Concentration and Saturated Vapor Concentration

From Figs 8 and 13, it was seen that both mist concentration and vapor deposition rate increase with saturated vapor pressure at pool temperature. These can well be explained when one consider the mist formation. Within the temperature boundary layer above pool surface, evaporated sodium vapor nucleate easily as they apart from the surface and were cooled with supersaturation larger than 30-50[1]. Thin nucleation zone is formed, therefore, above pool surface and, within this zone, no mists could be found[1]. Thus, evaporation rate of vapor ε could be expressed as follows as an approximation

$$\varepsilon = D\frac{P_s - P_\infty}{\delta} \tag{43}$$

where Ps; saturated vapor concentration at pool surface.

P_∞; suturated vapor concentration at nucleation zone.

δ; hight of nucleation zone from pool surface

In this, concentration P_∞ at nucleation zone is negligibly small compared to Ps at pool surface. Thus, source term for sodium mists in cover gas space become proportional to vapor concentration Ps at pool temperature and this would result as shown in Fig 8 and 13.

6 Conclusion

Sodium vapor deposition rate on annular surface were experimentaly determined, and were compared with numericaly calculated vapor condensation rate based on saturated vapor transfer by cover gas natural convection. In addition, sodium mists concentration in Ar cover gas space were experimentaly determined using the similar geometry used for vapor deposition experiment. With these, following conclusion were infered and derived

(1) Vapor deposition on annular surface was mainly due to mists transfer, and experimental deposition rate was about 100 times larger than saturated vapor condensation rate.

(2) Experimental mists concentration were between 0.3-4 g/m^3, and these values are about 200 times higher than saturated vapor concentration in cover gas.

(3) Both vapor deposition rate and mist concentration increase with saturated vapor pressure at pool temperature.

For further accurate evaluation and analysis of vapor deposition data, investigation on behavior of mist in cover gas space is required.

Acknowledgement

The first author express his deep gratitude to Dr. T. Kumada, Associate Proffessor of Hokkaido University, for his helpful advice and suggestion throughout the work. Thanks are also given to Dr. G. Nishio of JAERI for his variable suggestion.

Literature Cited

(1) Kumada.T, Ishiguro.R and Shimizu.T., 13th Symp. Heat Transfer. Japan (in Japanese), Preprint, D305, 505, May 1976.

(2) Honesty.C.C and Wolson.R.D., ANL-7957, pp 33-36, 1972.

(3) Takahashi.K., "Kiso Aerosol Kogaku (in Japanese)" Yokendo Japan. 1972.

(4) Wilke.C.R and Lee.C.Y., Ind. Eng. Chem., 47, 6, pp 1253-1257, 1955.

(5) Torrance.K.E and Rockett.J.A., J. Fluid Mech., 36, part 1, pp 33-54, 1970.

(6) Abe.T and Ishiguro.R., Nihon Kikaigakkai Ronbunshu (in Japanese), 41, No 352, 3577, 1970.

(7) Sheth.A., ANL-75-11, March 1975.